Hindered surface diffusion of bonded molecular clusters mediated by surface defects

William S. Huxter [1,*] Chandra Veer Singh [1,2] and Jun Nogami [1,†]

[1]*Department of Materials Science and Engineering, University of Toronto, 184 College Street, Toronto, Ontario, Canada, M5S 3E4*

[2]*Department of Mechanical and Industrial Engineering, University of Toronto, 5 King's College Road, Toronto, Ontario, Canada, M5S 3G8*

(Received 29 August 2019; revised 21 July 2020; accepted 20 August 2020; published 23 September 2020)

The design of low dimensional materials through surface assisted self-assembly requires a better understanding of the factors that limit and control surface diffusion. We reveal how substrate surface defects hinder the mobility of submonolayer organic adsorbates on a metal surface with the model CuPc/Cu(111) system. Postdeposition annealing bonds CuPc molecules into dendritelike clusters that are often mobile at room temperature. Surface defects on Cu(111) create energetic barriers that prevent CuPc cluster motion on the metal surface. This phenomenon was unveiled by the motion of small clusters that show rigid-body diffusion solely in the available space in between defects. When clusters are sufficiently surrounded by defects, they become completely pinned in place and become immobilized.

DOI: 10.1103/PhysRevMaterials.4.093401

I. INTRODUCTION

The synthesis of low dimensional materials from molecular building blocks is a rich and promising area of molecular nanotechnology [1,2]. A common route for material synthesis involves facilitating covalent bonding between precursor molecules on an atomically flat substrate through an annealing treatment. The substrate, often a transition metal, assists in the reaction by limiting the adsorbed molecules to the two-dimensional (2D) surface and may act as a catalyst by providing adatoms for reaction intermediates [3–5]. One practical challenge with these coupled self-assemblies lies in determining the fundamental mechanisms and interactions that are important in the design of the formed polymer or oligomer. Discovering what controls these factors may lead to new physical and chemical insights in low dimensional systems. For instance, it has been demonstrated that polymer/oligomer morphology is greatly affected by changes in adsorbate surface mobility [6,7], temperature-dependent bonding mechanisms [8,9], and substrate temperature during precursor deposition [10].

Point defects on the substrate surface are often overlooked in this synthesis process. While experimental preparation techniques have advanced to generate nearly ideal substrates, surface defects are almost always unavoidable. These defects may physically and chemically interfere with precursors and modify reaction mechanisms. Thus, these defects merit a careful investigation. In this paper, we investigate the role of surface defects through the study of annealed submonolayer (ML) copper-phthalocyanine (CuPc) on Cu(111) with scanning tunneling microscopy (STM) and density functional theory (DFT) stimulations.

CuPc/Cu(111) is a model 2D π-conjugated molecule-metal system. Such systems form a variety of 2D structures [11,12] and have applications ranging from catalysis [13] to molecular spintronics [14,15] and organic electronic devices [16,17]. Specifically, the CuPc/Cu(111) system has been extensively characterized across many techniques from sub-ML to multilayer coverage across a large temperature range [18–30]. Room-temperature (RT) STM experiments show that CuPc is highly mobile on noble-metal (111) surfaces at coverages under 1 ML [21,28,29,31]. The STM tip measures the time-averaged motion of CuPc across the surface as a diffusive background feature, as well as interference patterns from CuPc scattering around surface defects and step edges. Similar metal-phthalocyanine (MePc)/metal systems [32–34] show evidence of C-C bond formation after annealing, however bond formation through annealing has yet to be investigated on CuPc/Cu(111).

We find that annealing CuPc on Cu(111) yields dendritelike clusters as a result of a dehydrogenation reaction that creates biphenyl links between molecules. CuPc appears to become immobilized after forming clusters, however, many smaller clusters diffuse and rotate on the Cu(111) terraces. Experimental observations and theoretical calculations demonstrate that clusters are immobilized by the energetic barriers created around surface defects that prevent CuPc diffusion. This reveals that the stochastic nature of surface defects can severely limit the cluster's surface mobility. Considering the significance of CuPc/Cu(111) as a prototypical system, we believe that these findings greatly add to the fundamental understanding of on-surface synthesis and may promote further studies of phthalocyanines, porphyrins, and other 2D π-conjugated molecules.

II. EXPERIMENTAL AND THEORETICAL DETAILS

Experiments were carried out in an RT ultrahigh vacuum (UHV) STM chamber with a base pressure of

*Present address: Department of Physics, ETH Zurich, Otto Stern Weg 1, 8093 Zurich, Switzerland.

†Corresponding author: jun.nogami@utoronto.ca

$\sim 3.0 \times 10^{-10}$ Torr. Sample cleaning is described in Ref. [35]. CuPc was evaporated from a sublimated purified CuPc powder inside a direct-current heated quartz Knudsen cell. Current controlled deposition was monitored by an *in situ* quartz crystal microbalance (QCM) and the deposition rate was measured to be $\sim$0.15 ML/min. Postdeposition annealing occurred at $\sim$573 K via a ceramic radiative heater placed on the back of the Cu(111) sample plate. This temperature was slightly higher than previously reported experiments on CuPc/Cu(111) that did not show bonding [22,23]. Postdeposition annealing times varied from 15 to 30 min. Images were collected with Pt-Ir tips in the constant current mode and postprocessed with WSxM [36].

DFT simulations were performed using VASP [37] with projector augmented-wave potentials [38,39], generalized gradient approximation (GGA)–Perdew-Burke-Ernzerhof functionals [40], and DFT-D3 and Becke-Jonson damping for van der Waals corrections [41,42]. Simulation details included a kinetic-energy cutoff of 500 eV and gamma point sampling (which is adequate due to the large supercells). Self-consistent calculations utilized a threshold of 10^{-4} eV/Å for force convergence and a threshold of 10^{-5} eV for total-energy convergence. Four different Cu(111) slabs were created for simulations with different CuPc/Cu(111) and CuPc-CuPc/Cu(111) geometries and interaction schemes. Slab details are included in Ref. [35], including a discussion about the electronic structure of CuPc and comparison with other GGA simulations [43]. STM simulations followed the Tersoff-Hamann theory [44].

III. RESULTS AND DISCUSSION

An example of covalently bonded CuPc clusters created at 0.25 ML is shown in Fig. 1(a). These dendritelike clusters are heavily branched, often extend across entire Cu(111) terraces, and are on the order of 50 CuPc molecules in size when not limited by step edges. Clusters are primarily formed out of two different intermolecular bonding orientations: a parallel orientation, shown in Fig. 1(b), where bonding lobes of the CuPc lie along parallel lines, and an angular orientation, shown in Fig. 1(c), where bonding lobes lie 120° apart. DFT simulations of these bonding arrangements are shown in Figs. 1(d)–1(g) and they strongly support our observation of C-C bond formation. STM simulations and Cu-Cu distances from DFT calculations match the experimental observations well. Additionally, the reduced C_{2v} symmetry of the adsorbed CuPc molecule is clearly visible. This symmetry is induced through interaction of the Cu(111) surface and can be observed as the bright and dark lobes seen on the CuPc molecules. C_{2v} symmetries of MePc molecules are consistent with previous observations across (111) metal surfaces [19,30,45]. Prior theoretical calculations [46,47] have shown that brighter lobes align with close-packed directions of the substrate. While the bonding lobes in Fig. 1(b) and the nonbonding lobes in Fig. 1(c) are slightly brighter, the opposite cases were also observed, albeit less frequently [35]. This suggests that CuPc orientation on the substrate has a negligible influence on the type of bond formed.

While each isoindole lobe of the CuPc molecule features two bonding sites on the peripheral carbon atoms, steric hindrance limits each lobe to one bond only. These bonding orientations match the structures observed previously on CuPc/Ag(111) [32], FePc/Cu(111) [33], and ZnPc/Cu(100) [34] (parallel bonding only) which suggests that the formation of the biphenyl link is minimally dependent on the choice of metal center and metal substrate. The biphenyl link bears a similarity to, but is different from, the bonding observed with annealed octaethyl-tetra-aza-porphyrin (OETAP) on Au(111) [10]. Post-deposition annealing transforms OETAP into phthalocyanine molecules which become bonded together through naphthalene links. These naphthalene links place the molecule centers closer together than biphenyl links and are inconsistent with our observations. Additionally, the benzene terminated lobes of CuPc are structurally and chemically different from the ethylene terminated lobes of OETAP which are required for creating the naphthalene links. Interestingly, the Au(111) surface reconstruction appears to spatially confine the annealed OETAP clusters

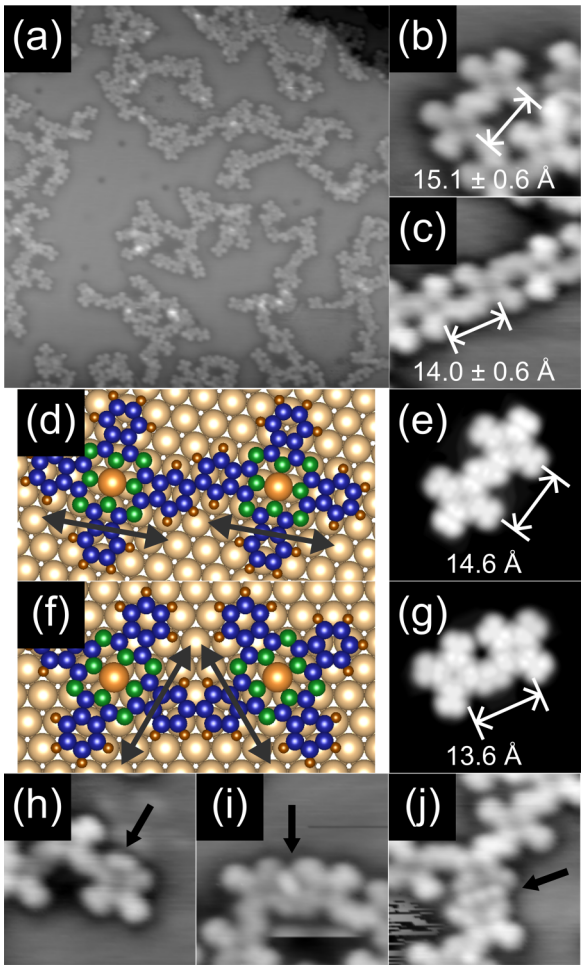

FIG. 1. (a) Annealed 0.25-ML CuPc on Cu(111) (500×500 Å^2). Specific parallel (b) and angular (c) bonding orientations (50×50 Å^2). Atomic model (d) and STM simulation (e) of parallel bonding. Atomic model (f) and STM simulation (g) of angular bonding. (h)–(j) Different CuPc-Cu adatom coordination structures (50×50 Å^2). STM simulations at +0.9 V. Imaged +0.9 V and 0.5 nA.

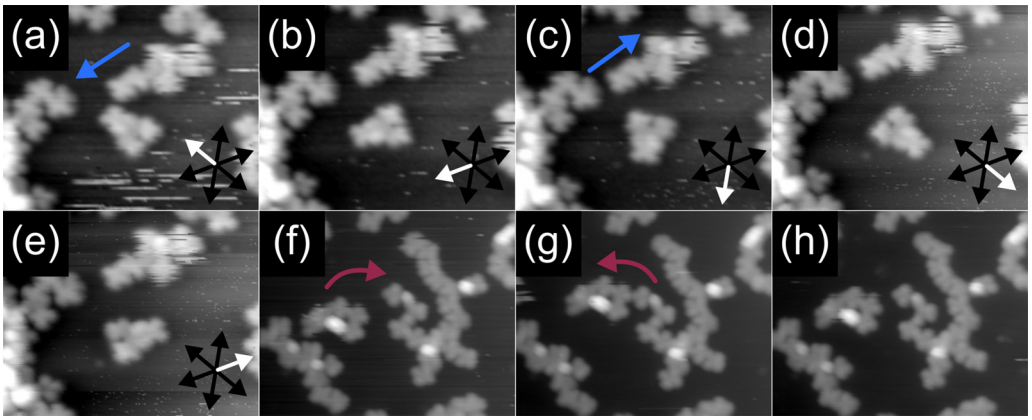

FIG. 2. 0.15-ML CuPc on Cu(111) with postdeposition annealing. (a)–(e) Rotational configurations of a CuPc cluster (−1.0 V, 0.5 nA, 200 × 160 Å^2). The stable positions are indicated by white and black arrows. Diffusion back and forth between different orientations was observed across 17 sequential images recorded over a 3.5-h period. Translations by another cluster are also indicated by blue arrows. (f)–(h) Interaction between different CuPc clusters across three sequential scans highlighted with red arrows (−1.1 V, 0.5 nA, 250 × 200 Å^2).

which preferentially grow in the fcc regions of the herringbone structure [10]. On Cu(111) the CuPc clusters show no preferred morphology and tend to grow in all directions.

In rare instances, CuPc-Cu adatom coordination was observed. Several seemingly hierarchical structures were formed as depicted in Figs. 1(h)–1(j). The lobes near Cu adatoms are adsorbed closer to the surface as they appear darker in STM images. It is likely that CuPc are stabilized by this interaction, similar to how single Ag adatoms have been shown to stabilize CuPc on Ag(100) [48] and to how other adsorbed molecules interact with Cu adatoms on Cu(111) and Cu(100) [49–56]. We do not believe this coordination is caused by the hydrogen lost during the dehydrogenation reaction since both atomic and molecular hydrogen would not stick to or interact with the Cu(111) surface within the relevant temperature range [57,58].

Different CuPc coverages were studied to measure changes in cluster size upon annealing. At 0.15 ML, many smaller clusters were observed (compared to 0.25 ML) that were spread evenly over the surface. The smallest resolvable cluster contained three CuPc molecules. Surprisingly, repeated STM scans (∼10 min per image) revealed rigid-body motion by a fraction of the clusters, including diffusion and rotations, as shown in Fig. 2. Cluster diffusion was observed to be as large as a several nanometers in between scans. Rotations, which were rarely observed, featured stable positions on the Cu surface that were roughly 60° apart [see Figs. 2(a)–2(e)]. This suggests that rotating clusters were aligning with close-packed directions. When mobile clusters interacted with immobile clusters, as in Figs. 2(f)–2(h), the CuPc-CuPc distances from the nearest interacting CuPc molecules were sufficiently large to conclude that they were not bonding to each other. Clusters bonded to CuPc at step edges as well as clusters with CuPc-Cu adatom coordination were observed to be immobile.

The observed cluster motion was varied and complex. Mobile clusters were sometimes well-resolved and other times noisy from scan to scan. Evidently, mobile clusters could be motionless or in motion while the STM tip was scanning directly above the cluster. In general, smaller clusters were more likely to be mobile. One possible explanation is that larger clusters diffuse at slower rates due to their size and eventually, at a threshold size, become too large to move. However, this does not explain why some very small clusters (<5 CuPc) were immobile yet many larger clusters (up to ∼20 CuPc) were mobile. Possibilities of tip induced effects, such as a chemisorption mechanism [26,59–61] or local electric fields [62], are not likely as motion was observed at both scanning biases and no voltage pulses were applied from the scanning tip.

It is already understood that CuPc molecules on clean Cu(111) are highly mobile at RT at sub-ML coverages, and do not appear in STM images at room temperature. At coverages approaching 1 ML, the presence of mobile CuPc becomes apparent as a smooth background that is higher than the bare substrate [31,63]. An ordered 2D CuPc phase only becomes apparent to STM as the coverage reaches 1 ML and the second layer of CuPc only begins to form once the first ML is completed [27]. Here, we additionally report that bonded CuPc molecules also remain mobile on the surface and that their diffusive behavior deviates from that of their single nonbonded counterparts.

To further understand cluster mobility, additional CuPc can be deposited on a surface with CuPc clusters without subsequent annealing. Thus, differences in mobility between clusters and single molecules is easily distinguishable in the same STM scan. Figure 3 displays the annealed 0.15-ML CuPc surface before and after adding an additional 0.15-ML CuPc without annealing. In Fig. 3(a) noisy streaks, which are topographically the same height as the immobile clusters, are indicated with white arrows. The diffuse background created by highly mobile CuPc in Fig. 3(b) sits at a lower topographic height and is considerably different than the noisy streaks in both STM scans (see Refs. [31,63] for more information about the diffusive background). We attribute the noisy streaks to CuPc clusters—possibly bonded CuPc pairs—that were moving too quickly to be fully resolved by the tip. These streaks appear brighter than the diffusive background because they are diffusing more slowly than individual CuPc molecules and therefore spend a larger amount of time under the STM tip.

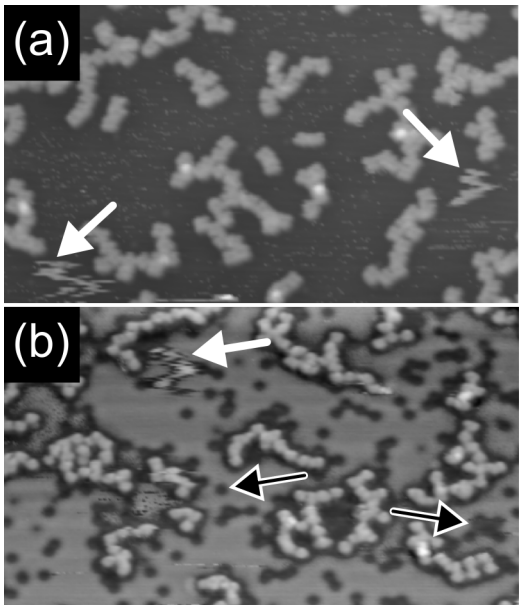

FIG. 3. Addition of 0.15-ML CuPc without annealing. (a) STM scan of annealed CuPc before additional deposition (−2.0 V, 0.1 nA, 600 × 350 Å^2). (b) STM scan after additional deposition of CuPc (−1.2 V, 0.5 nA, 600 × 350 Å^2). White arrows indicate mobile clusters and black arrows indicate substrate surface defects.

Single CuPc molecules also scatter off CuPc clusters. Regions devoid of the diffusive background around surface defects are also found around clusters. A few surface defects are indicated in Fig. 3(b) with black arrows. Regions between defects that CuPc molecules are physically incapable of occupying show no diffusive background, giving the appearance of extended defect structures (more details in Ref. [35]).

In Figs. 2 and 3 we have observed two types of motion: (1) highly mobile single CuPc molecules that appear as a diffusive background, and (2) bonded CuPc clusters that can either be unresolvable in a single image (streaky) or fully resolved from image to image. While the inability to change the operating temperature of the STM limits our ability to measure diffusion parameters (diffusion prefactor D_0 and activation energy E_A), we can estimate and compare the diffusion speeds of CuPc molecules and CuPc clusters (calculation details in Ref. [35]). Additionally, measured displacements can lead to estimates for the diffusion coefficient D [$D = D_0 \exp(-E_A/k_B T)$] at RT. Single CuPc molecules must be moving at speeds at least on the order of 1.5×10^3 nm/s with $D \sim 10^{-11}$ cm^2/s, given our tip dwell time and the inability to resolve any molecular features. The clusters, however, must be moving significantly slower. Clusters that produce noisy streaks (such as the streaks denoted by white arrows in Fig. 3) can be moving as slowly as 1.2×10^0 nm/s and clusters that only appear to be moving in between scans (such as the clusters in Fig. 2) can be moving as slow as 10^{-2} to 10^{-3} nm/s. These values correspond to $D \sim 10^{-14}$ cm^2/s to 10^{-17}cm^2/s, which is three to six orders of magnitude smaller. It should be noted that these estimates are only lower bounds and that it is possible that some clusters are moving faster. It is difficult to observe motion on the order $10^1 - 10^2$ nm/s as that is comparable to our tip scanning speed. We also find that there is a weak correlation between the size of the cluster and the motion; larger clusters appear to move more slowly than smaller clusters.

A series of DFT simulations provides insights into the behavior of sub-ML CuPc on Cu(111) by measuring the change in CuPc adsorption energy across a variety of CuPc/substrate interactions. Figure 4 displays the clear trend that CuPc is further stabilized by increasing the interaction with substrate atoms and is less stable upon increasing CuPc-CuPc interaction. A full description of the simulation details are found in Ref. [35]. When CuPc interacts at or near a step edge the adsorption energy is ∼1 eV more stable. Isolated CuPc and monolayer CuPc occupy a range of roughly 0.48 eV due to the different possible positions of the molecules on the Cu(111) surface. This value represents an upper bound for the diffusion barrier of CuPc on Cu(111) [35]. The adsorption energy begins to quickly increase as CuPc lobes are removed

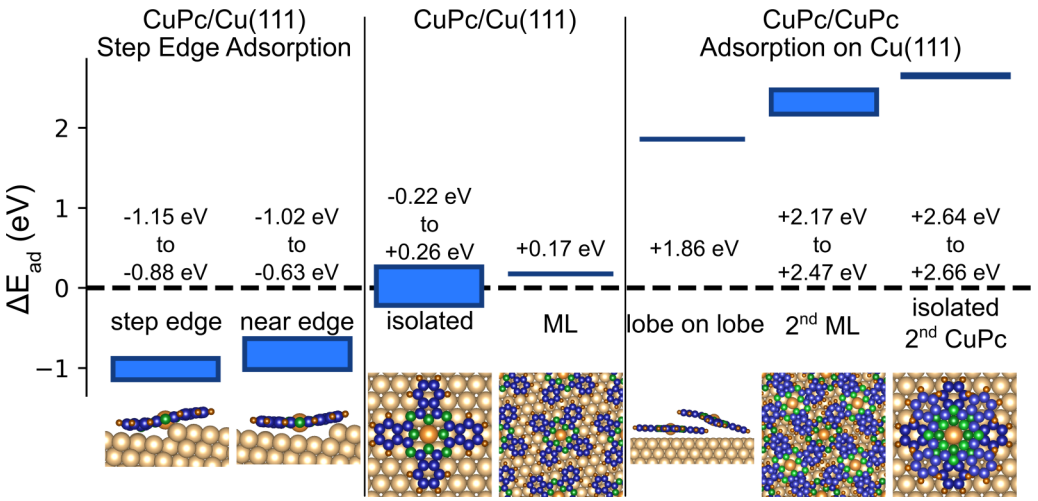

FIG. 4. Relative stability of CuPc across different interaction schemes. CuPc adsorption on Cu(111) is used as the reference energy. The energy ranges come from taking the range of adsorption energies from several different geometries (details in Ref. [35]). Negative energies are more stable.

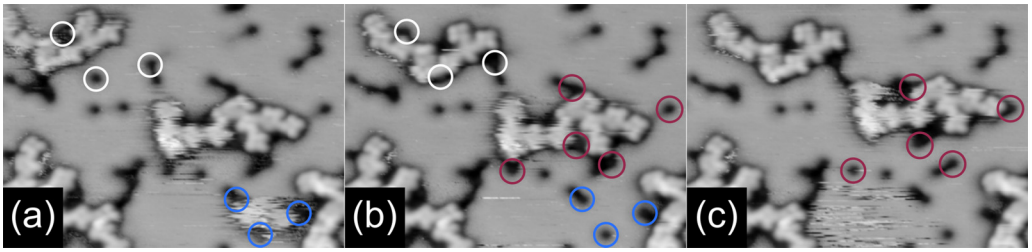

FIG. 5. (a)–(c) Sequential scans that track mobile cluster movement. From panel (a) to (b) the topmost cluster moves until it is pinned by surface defects outlined in white. Another cluster, enclosed by defects outlined with blue, disappears in panel (b). From panel (b) to (c) motion of another cluster is hindered by defects outlined in red. All imaged at −1.0 V, 0.4 nA, 300 × 180 Å^2.

from the Cu(111) surface and forced to interact with other CuPc. CuPc in the second ML are ∼2.5 eV less stable than in the first ML.

These energies provide results consistent with the experimental observations. CuPc deposited onto Cu(111) at RT can further increase its stability by adsorbing at step edges [which has been previously observed on CuPc/Cu(111) [26,27], CuPc/Au(111) [64], and FePc/Cu(111) [65]]. The ∼1-eV increase in stability is larger than the thermal energy of CuPc as the molecules do not desorb from the step edges. When CuPc is deposited onto the postannealed surface (with bonded CuPc clusters), no single CuPc molecules remain on top of clusters. If CuPc were to land on top of a cluster, the CuPc would increase its energetic stability by transitioning off the cluster and onto the available Cu(111) surface.

Repeated STM scans of the cluster plus single molecule surface, shown in Fig. 5 clearly show that the highlighted surface defects hinder cluster mobility The clusters surrounded by defects outlined in white and red move within their defect-free region from scan to scan and never move over any defects. The cluster surrounded by defects outlined in blue moves very quickly inside its defect-free region, then appears to escape that space in Fig. 5(b) as the noisy streaks indicative of the cluster disappears. It is likely that this cluster moved through the two leftmost highlighted defects as a characteristic noisy streak is observed to the left of those defects in Fig. 5(c). The same type of behavior is also shown with the mobile cluster indicated by the white arrow in Fig. 3(b).

Surface defects acting as pinning sites for CuPc cluster motion provide an adequate explanation for the observed cluster motion. Very small clusters should almost always be mobile as they would be able to move between most surface defects. If a cluster is surrounded by a few defects, such as those surrounded by highlighted defects in Fig. 5, it is possible that motion is restricted to a small area. If surrounded by enough surface defects, the entire cluster becomes immobilized. As the cluster size increases, such as when annealing at higher CuPc coverages, it is more likely that clusters are surrounded by enough surface defects to become immobilized. Due to the stochastic nature of surface defects, it is possible that some larger clusters remain mobile while smaller clusters are immobile. It is also likely that larger clusters naturally diffuse more slowly on the surface. However, surface defects, step edges, and Cu adatom coordination appear to be the most important factors responsible for cluster immobilization. The importance of surface defects revealed here may have significant consequences across a large variety of molecule/metal systems. This mechanism may explain the mobility (and lack of mobility) in other cases of rigid-body diffusion of bonded molecules [10,66], especially those where the mobility of the molecular cluster largely deviates from that of individual molecules.

Auger spectroscopy on Cu(111) single crystals prepared in a similar manner to our samples has revealed that sulfur is likely the primary surface contaminant [67]. Annealing cycles used in sample preparation enables sulfur to diffuse from the bulk to the surface. This specific phenomenon has been used previously to study S adatoms on Cu [68,69]. Figures 6(a) and 6(b) display typical STM images of surface defects on Cu(111) before and after a tip change. The observed morphology is characteristic of STM images of single sulfur atoms on noble-metal surfaces. Specifically, the protrusions imaged

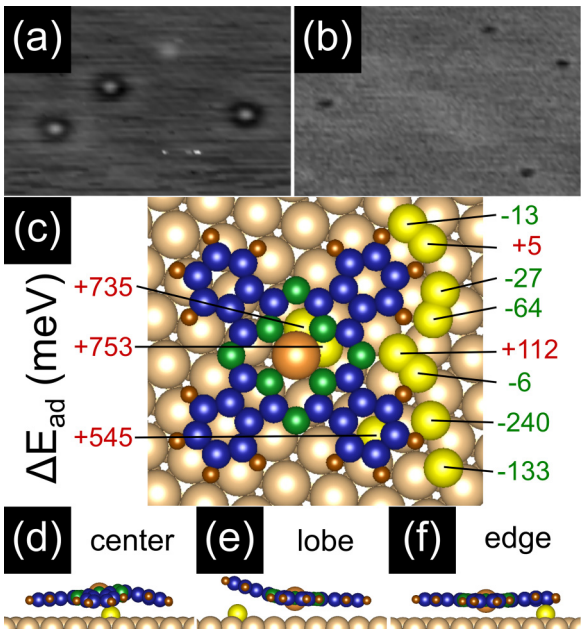

FIG. 6. Surface defects on Cu(111) before (a) and after (b) a tip change (−1,2 V, 0.2 nA, 120 × 80 Å^2) (c) Relative adsorption energies of CuPc near and on top of S defects. (d)–(f) Three relaxed geometries of CuPc by S on Cu(111).

in Fig. 6(a) have a height of ∼0.016 nm and a full width at half max of ∼0.36 nm, similar to the values of isolated S on Cu(100) [70] and S on Au(111) [71]. The imaged defects do not appear like the Cu_2S_3 complexes or sulfur induced reconstructed steps observed on Cu(111) [72,73]. Given the appearance of the defects in our data, we assume that isolated sulfur atoms are the primary surface defect responsible for hindering cluster motion.

DFT simulations of this type of defect reveal how cluster motion is hindered. Eleven different fcc and hcp sites were populated with a sulfur atom either underneath or beside an isolated CuPc molecule. The locations of these sites relative to the adsorbed CuPc and the changes in adsorption energy, ΔE_{ad}, are shown in Fig. 6(c). Positive values indicate a less favorable adsorption configuration. Figures 6(d)–6(f) display the relaxed geometry of a few cases. Sulfur adatoms placed near the edge of the lobes show a slight decrease in adsorption energy. However, these small changes are mostly comparable to changes in energy as CuPc moves across the Cu(111) surface and activation barriers for MePc diffusion on Ag(100) [74,75] and on Au(111) [76]. Thus, sulfur near the edges of CuPc minimally affects the molecule. Sulfur underneath CuPc however, is not favorable as it interferes with the adsorbate-substrate interaction. The unfavorable adsorption of CuPc on top of sulfur demonstrates that CuPc molecules (and clusters) experience a significant energetic barrier as they try to move over a surface defect. In the case of single molecules, this produces scattering patterns [26,27]. In the case of bonded CuPc clusters, this hinders motion in the *xy* plane and can effectively trap clusters.

IV. CONCLUSION

A mechanism is presented whereby molecular clusters are immobilized by substrate surface defects. Dendritelike CuPc clusters reveal complex rigid-body mobility (and immobility) on the Cu(111) surface that is, to a first-order approximation, cluster size dependent but also subject to stochastic randomness from the distribution of substrate surface defects. Surface defect pinning, in combination with substrate step edges, native adatoms coordination, and size dependent diffusion constants, provides a complete picture of how and why mobile precursor molecules may combine into immobile polymers and oligomers.

ACKNOWLEDGMENTS

This research was possible through the support provided by Natural Sciences and Engineering Research Council of Canada (NSERC), Grants No. RGPIN-2017-06069 and No. RGPIN-2018-04642. Hart Professorship, and the University of Toronto. Computations were conducted through the Compute Canada facilities, namely the Niagara cluster.

[1] G. M. Whitesides, J. P. Mathias, and C. T. Seto, Science **254**, 1312 (1991).
[2] J. V. Barth, G. Costantini, and K. Kern, Nature (London) **437**, 671 (2005).
[3] L. Bartels, Nat. Chem. **22**, 87 (2010).
[4] G. Franc and A. Gourdon, Phys. Chem. Chem. Phys. **13**, 14283 (2011).
[5] S. Clair and D. G. de Oteyza, Chem. Rev. **119**, 4717 (2019).
[6] M. Bieri, M.-T. Nguyen, O. Gröning, J. Cai, M. Treier, K. Aït-Mansour, P. Ruffieux, C. A. Pignedoli, D. Passerone, M. Kastler, K. Müllen, and R. Fasel, J. Am. Chem. Soc. **132**, 16669 (2010).
[7] A. L. Pinardi *et al.*, ACS Nano **7**, 3676 (2013).
[8] L. Lafferentz, V. Eberhardt, C. Dri, C. Africh, G. Comelli, F. Esch, S. Hecht, and L. Grill, Nat. Chem. **4**, 215 (2012).
[9] Q. Li *et al.*, J. Am. Chem. Soc. **138**, 2809 (2016).
[10] B. Cirera, N. Giménez-Agulló, J. Björk, F. Martínez-Peña, A. Martin-Jimenez, J. Rodriguez-Fernandez, A. M. Pizarro, R. Otero, J. M. Gallego, P. Ballester, J. R. Galan-Mascaros, and D. Ecija, Nat. Commun. **7**, 11002 (2016).
[11] J. M. Gottfried, Surf. Sci. Rep. **70**, 259 (2015).
[12] W. Auwärter, D. Écija, F. Klappenberger, and J. V. Barth, Nat. Chem. **7**, 105 (2015).
[13] A. B. Sorokin, Chem. Rev. **113**, 8152 (2013).
[14] S. Sanvito, Chem. Soc. Rev. **40**, 3336 (2011).
[15] R. Geng, H. M. Luong, T. T. Daugherty, L. Hornak, and T. D. Nguyen, J. Sci. Adv. Mater. Dev. **1**, 256 (2016).
[16] G. Bottari, G. de la Torre, D. M. Guldi, and T. Torres, Chem. Rev. **110**, 6768 (2010).
[17] O. A. Melville, B. H. Lessard, and T. P. Bender, ACS Appl. Mater. Interfaces **7**, 13105 (2015).
[18] J. C. Buchholz and G. A. Somorjai, J. Chem. Phys. **66**, 573 (1977).
[19] H. Karacuban, M. Lange, J. Schaffert, O. Weingart, T. Wagner, and R. Möller, Surf. Sci. **603**, L39 (2009).
[20] D. G. de Oteyza *et al.*, J. Chem. Phys. **133**, 214703 (2010).
[21] I. Kröger, B. Stadtmüller, C. Wagner, C. Weiss, R. Temriov, F. S. Tautz, and C. Kumpf, J. Chem. Phys. **135**, 234703 (2011).
[22] B. Stadtmüller, I. Kröger, F. Reinert, and C. Kumpf, Phys. Rev. B **83**, 085416 (2011).
[23] I. Kröger, B. Stadtmüller, C. Kleimann, P. Rajput, and C. Kumpf, Phys. Rev. B **83**, 195414 (2011).
[24] J. Schaffert, M. C. Cottin, A. Sonntag, C. A. Bobisch, R. Möller, J.-P. Gauyacq, and N. Lorente, Phys. Rev. B **88**, 075410 (2013).
[25] J. Schaffert, M. C. Cottin, A. Sonntag, H. Karacuban, C. A. Bobisch, N. Lorente, J.-P. Gauyacq, and R. Möller, Nat. Mater. **12**, 223 (2013).
[26] T. J. Z. Stock and J. Nogami, Appl. Phys. Lett. **104**, 071601 (2014).
[27] T. J. Z. Stock and J. Nogami, Surf. Sci. **637-638**, 132 (2015).
[28] T. J. Z. Stock, Ph.D. thesis, University of Toronto, 2015.
[29] M. Mehdizadeh, M.A.Sc. thesis, University of Toronto, 2017.
[30] S. Fremy-Koch, A. Sadeghi, R. Pawlak, S. Kawai, A. Baratoff, S. Goedecker, E. Meyer, and T. Glatzel, Phys. Rev. B **100**, 155427 (2019).
[31] G. Antczak, K. Boom, and K. Morgenstern, J. Phys. Chem. C **121**, 542 (2017).

[32] K. Manandhar, T. Ellis, K. T. Park, T. Cai, Z. Song, and J. Hrbek, Surf. Sci. **601**, 3623 (2007).

[33] O. Snezhkova *et al.*, J. Chem. Phys. **144**, 094702 (2016).

[34] F. Chen *et al.*, Appl. Phys. Lett. **100**, 081602 (2012).

[35] See Supplemental Material at http://link.aps.org/supplemental/10.1103/PhysRevMaterials.4.093401 for more information on CuPc clusters, cluster statics, DFT simulations, and diffusion speed estimation.

[36] I. Horcas, R. Fernández, J. M. Gómez-Rodríguez, J. Colchero, J. Gómez-Herrero, and A. M. Baro, Rev. Sci. Instrum. **78**, 013705 (2007).

[37] G. Kresse and J. Furthmuller, Phys. Rev. B **54**, 11169 (1996).

[38] P. E. Blöchl, Phys. Rev. B **50**, 17953 (1994).

[39] G. Kresse and D. Joubert, Phys. Rev. B **59**, 1758 (1999).

[40] J. P. Perdew, K. Burke, and M. Ernzerhof, Phys. Rev. Lett. **77**, 3865 (1996).

[41] S. Grimme, J. Antony, S. Ehrlich, and H. Krieg, J. Chem. Phys. **132**, 154104 (2010).

[42] S. Grimme, S. Ehrlich, and L. Goerigk, J. Comput. Chem. **32**, 1456 (2011).

[43] N. Marom, O. Hod, G. E. Scuseria, and L. Kronik, J. Chem. Phys. **128**, 164107 (2008).

[44] J. Tersoff and D. R. Hamann, Phys. Rev. B **31**, 805 (1985).

[45] S.-H. Chang, S. Kuck, J. Brede, L. Lichtenstein, G. Hoffmann, and R. Wiesendanger, Phys. Rev. B **78**, 233409 (2008).

[46] J. D. Baran and J. A. Larsson, J. Phys. Chem. C **117**, 23887 (2013).

[47] D. Lüftner, M. Milko, S. Huppmann, M. Scholz, N. Ngyuen, M. Wießner, A. Schöll, F. Reinert, and P. Puschniga, J. Electron. Spectrosc. **195**, 293 (2014).

[48] G. Antczak, W. Kamiński, and K. Morgenstern, J. Phys. Chem. C **119**, 1442 (2014).

[49] M. Matena, T. Riehm, M. Stöhr, T. A. Jung, and L. H. Gade, Angew. Chem. Int. Ed. **47**, 2414 (2008).

[50] J. Björk, M. Matena, M. S. Dyer, M. Enache, J. Lobo-Checa, L. H. Gade, T. A. Jung, M. Stöhr, and M. Mats Persson, Phys. Chem. Chem. Phys. **12**, 8815 (2010).

[51] M.-A. Dubois, O. Guillermet, S. Gauthier, G. Zhan, Y. Makoudi, F. Palmino, X. Bouju, and A. Rochefort, Phys. Chem. Chem. Phys. **20**, 15350 (2018).

[52] M. Lischka, R. Dong, M. Wang, N. Martsinovich, M. Fritton, L. Grossmann, W. M. Heckl, X. Feng, and M. Lackinger, Chem. Eur. J. **25**, 1975 (2019).

[53] N. P. Guisinger, A. J. Mannix, R. B. Rankin, B. Kiraly, J. A. Phillips, S. B. Darling, B. L. Fisher, M. C. Hersam, and E. V. Iski, Adv. Mater. Interfaces **6**, 1900021 (2019).

[54] N. Lin, A. Dmitriev, J. Weckesser, J. V. Barth, and K. Kern, Angew. Chem. Int. Ed. **41**, 4779 (2002).

[55] T. Classen, G. Fratesi, G. Costantini, S. Fabris, F. L. Stadler, C. Kim, S. de Gironcoli, S. Baroni, and K. Kern, Angew. Chem. Int. Ed. **44**, 6142 (2005).

[56] S. L. Tait, A. Langner, N. Lin, S. Stepanow, C. Rajadurai, M. Ruben, and K. Kern, J. Phys. Chem. C **111**, 10982 (2007).

[57] G. Anger, A. Winkler, and K. D. Rendulic, Surf. Sci. **220**, 1 (1989).

[58] K. Mudiyanselage, Y. Yang, F. M. Hoffmann, O. J. Furlong, J. Hrbek, M. G. White, P. Liu, and D. J. Stacchiola, J. Chem. Phys. **139**, 044712 (2013).

[59] Y. C. Jeong, S. Y. Song, Y. Kim, Y. Oh, J. Kang, and J. Seo, J. Phys. Chem. C **119**, 27721 (2015).

[60] A. Zhao *et al.*, Science **309**, 1542 (2005).

[61] L. Chen, H. Li, and A. T. S. Wee, ACS Nano **3**, 3684 (2009).

[62] K. Nagaoka, S. Yaginuma, and T. Nakayama, Jpn. J. Appl. Phys. **57**, 020301 (2018).

[63] P. Matvija, F. Rozbořilm, P. Sobotík, I. Ošťádal, and P. Kocán, J. Phys. Chem. Lett. **8**, 4268 (2017).

[64] R. Sk, S. Arra, B. Dhara, J. S. Miller, M. Kabir, and A. Deshpande, J. Phys. Chem. C **122**, 11848 (2018).

[65] L. Zhang *et al.*, J. Phys. Chem. C **115**, 10791 (2011).

[66] M. In't Veld, P. Iavicoli, S. Haq, D. B. Amabilino, and R. Raval, Chem. Commun. **13**, 1536 (2008).

[67] B. J. Hinch, J. W. M. Frenken, G. Zhang, and J. P. Toennies, Surf. Sci. **259**, 288 (1991).

[68] J. C. Boulliard and M. P. Sotto, Surf. Sci. **195**, 255 (1988).

[69] S. Rousset, S. Gauthier, O. Siboulet, W. Sacks, M. Belin, and J. Klein, Phys. Rev. Lett. **63**, 1265 (1989).

[70] H. Walen, D.-J. Liu, J. Oh, H. J. Yang, P. M. Spurgeon, Y. Kim, and P. A. Thiel, J. Phys. Chem. B **122**, 963 (2017).

[71] H. Walen, D.-J. Liu, J. Oh, H. Lim, J. W. Evans, Y. Kim, and P. A. Thiel, J. Chem. Phys. **143**, 014704 (2015).

[72] H. Walen, D.-J. Liu, J. Oh, H. Lim, J. W. Evans, C. M. Aikens, Y. Kim, and P. A. Thiel, Phys. Rev. B **91**, 045426 (2015).

[73] H. Walen, D.-J. Liu, J. Oh, H. Lim, J. W. Evans, Y. Kim, and P. A. Thiel, J. Chem. Phys **142**, 194711 (2015).

[74] G. y. Antczak, W. Kamiński, A. Sabik, C. Zaum, and K. Morgenstern, J. Am. Chem. Soc. **137**, 14920 (2015).

[75] J. Ikonomov, P. Bach, R. Merkel, and M. Sokolowski, Phys. Rev. B **81**, 161412(R) (2010).

[76] L. Buimaga-Iarinca and C. Morari, Sci. Rep. **8**, 12728 (2018).